Chemistry & Biology, Vol. 12, 811–823, July, 2005, ©2005 Elsevier Ltd All rights reserved. DOI 10.1016/j.chembiol.2005.05.011

Defining Cdk5 Ligand Chemical Space with Small Molecule Inhibitors of Tau Phosphorylation

Jae Suk Ahn,[1,5] Mala L. Radhakrishnan,[2] Marina Mapelli,[4] Sungwoon Choi,[1] Bruce Tidor,[3] Gregory D. Cuny,[1] Andrea Musacchio,[4] Li-An Yeh,[1,6] and Kenneth S. Kosik[1,7,*]

[1]Department of Neurology and Laboratory for Drug Discovery in Neurodegeneration
Brigham and Women's Hospital
Harvard Medical School
Boston, Massachusetts 02115
[2]Computer Science and Artificial Intelligence Laboratory
Department of Chemistry
[3]Computer Science and Artificial Intelligence Laboratory
Biological Engineering Division
Department of Electrical Engineering and Computer Science
Massachusetts Institute of Technology
Cambridge, Massachusetts 02139
[4]Structural Biology Unit
Department of Experimental Oncology
European Institute of Oncology
20141 Milan
Italy

Summary

Cyclin-dependent kinase 5 (Cdk5) is widely viewed as a possible target for a wide variety of neurological disorders. One pathological role attributed to Cdk5 is the abnormal phosphorylation of tau that may lead to the neuronal inclusions known as neurofibrillary tangles. A high through-put screen for inhibitors of Cdk5-mediated phosphorylation of tau resulted in three compounds with distinct mechanisms of action. One compound is competitive with ATP and has a high affinity for the Cdk5 ATP binding pocket. The second compound also competes with ATP, is non-competitive with tau, and (uniquely among this class of inhibitors) displaces adjacent amino acid residues to make room for the nitrophenyl group. A third compound did not compete with ATP, but did compete with tau at low concentrations of tau. The SAR and charge optimization derived from cocrystals of the two ATP competitors along with cocrystals of three other ATP competitors map out the importance of filling and properly charging different regions of the ATP binding pocket. Taken together, this analysis shows how the structure of Cdk5 constrains the space of potential inhibitors and reveals a pocket unfilled in all of the structures. These leads could be a starting point for structure-based drug design of more potent and selective inhibitors.

*Correspondence: kosik@lifesci.ucsb.edu
[5]Present address: Department of Pathology, College of Physicians and Surgeons, Columbia University, New York, New York 10032.
[6]Present address: Eli Lilly & Company, Lilly Corporate Center, Indianapolis, Indiana 46285.
[7]Present address: Neuroscience Research Institute, University of California, Santa Barbara, Santa Barbara, California 93106.

Introduction

Cdk5 is a member of a family of proline-directed serine/threonine kinases that is primarily active in the nervous system [1] and is essential for the development of the nervous system [2]. This kinase has 60% homology to human Cdk2 and cell division cycle kinase 2 (CDK1) [3–5]. In contrast to other members of the cyclin-dependent kinase family, Cdk5 does not mediate progression through the cell cycle. Rather, its activity is found predominantly in postmitotic neurons [6]. Although Cdk5 is expressed in many tissues, the basis for its localized activity is the restricted expression of the activators p35 and p39 [7]. A large body of data supports a role for this kinase in the pathogenesis of Alzheimer's disease (AD), amyotrophic lateral sclerosis (ALS), Parkinson's disease, Niemann-Pick type C disease, and ischemia [8–12]. However, controversy still exists as to the exact role of Cdk5 in these diseases [13].

The multiple disease phenotypes to which Cdk5 is thought to contribute are based on the large number of Cdk5 substrates. For example, phosphorylation of the NR2A subunit of the NMDA receptor by Cdk5 was shown to be responsible for hippocampal CA1 cell death after transient forebrain ischemia [12]. As a tau kinase [14, 15], Cdk5 has been implicated in the pathogenesis of the Alzheimer neurofibrillary tangles (NFTs) [16, 17], which are composed mainly of hyperphosphorylated tau aggregates. Strong support for assigning a role to Cdk5 comes from studies in transgenic mice [18, 19]. An attractive proposed mechanism for increased Cdk5 activity is an excessive upregulation of the Cdk5 activators following their truncation and release of the active complex from a membranous compartment [20]. The activators, p25 and p29, are proteolytic products containing the C-terminal portion of p35 and p39, respectively. p25, produced by calpain cleavage of p35 between residues 98 and 99 upon neurotoxic insults [21, 22], is fully capable of activating Cdk5. In addition, p25 is more stable than p35 and dissociates from its membrane attachment site to the cytosol [20].

The crystal structure of the Cdk5/p25 complex has clarified the mechanism of Cdk5 activation by p25 [23]. In general, Cdk activation requires a dual mechanism: binding of the cyclin box fold (CBF) region of the cyclins and the phosphorylation of Thr^{160} or Thr^{161} in the activation loop (also known as T-loop) by the Cdk-activating kinase [24]. In contrast, the Cdk5 activator, p25, contains a highly divergent CBF domain, which elicits an active conformation of CDK5 in the absence of phosphorylation [23]. Essentially, p25 tethers the T-loop of CDK5 into its active position.

Several classes of chemical inhibitors for Cdk have been reviewed [25]. Generally, these small molecules

compete with ATP and have IC_{50} values in the micromolar range [26–33]. Hymenialdisine inhibits in vivo phosphorylation of tau at AD-specific sites in cultured insect cells [34]. Alsterpaullone, a selective inhibitor for Cdk5 and GSK (glycogen synthetase kinase), inhibits the in vivo phosphorylation of tau at AD-specific sites in an insect cell line model and DARRP-32 phosphorylation in mouse striatum slices [31]. Some of the inhibitors have been cocrystalized with Cdk2 [35–37]. Recently, data on the crystal structure of active Cdk5/p25 kinase complexed with three inhibitor moieties, (R)-roscovitine, aloisine-A [32], and indirubin-3′-oxime [38], have been reported [39]. These chemical species inhibit catalytic activity by binding to the conserved ATP binding pocket.

Here we report the discovery of three small molecule Cdk5 inhibitors. Each of them has a distinct mechanism of action. Together they suggest novel opportunities for the design of compounds that could selectively inhibit Cdk5.

Results

Identification of Cdk5 Inhibitors and Their Inhibitor Kinetics

We previously configured a high-throughput assay to screen for inhibitors of tau phosphorylation at sites 396 and 404 mediated by Cdk5 [40]. A low concentration of full-length recombinant tau (0.1 μM) and a high concentration of ATP (200 μM) were used for the screen. The degree of tau phosphorylation was determined using PHF-1 antibody, which recognizes phosphorylation at serine 396 and serine 404. By performing the screen at the relatively high ATP concentration of 200 μM, inhibitors with a variety of kinetic properties emerged.

Various computational filters were applied to select compounds for the chemical library with an increased probability of oral bioavailability and blood brain barrier (BBB) penetration, which includes calculations of polar surface area (a physico-chemical descriptor that strongly correlates with oral bioavailability and the ability to cross the BBB), Lipinski's "rule of five," and other desirability filters. All compounds in the collection were plated in 384-well plates. Approximately 58,000 compounds were screened. This portion of the compound library consists of compounds purchased from eight primary vendors: Maybridge (9,000), Peakdale (3,000), Bionet (5,000), CEREP (4,800), ChemDiv (30,000), Prestwick collection of FDA-approved drugs (640), a natural product collection from Specs (480), and a tetrapeptide collection from Advanced Syntech (4,100), as well as 850 compounds from various academic labs and 595 unique compounds synthesized in-house. The hit rate after confirmation was 0.5% and the top three, based on their structure and IC_{50}, represent three major classes: a xanthen-9-one natural product bellidin, compound **1.0**, a 4-aminothiazole, compound **2.0**, and a 2,3-dihydro-1H-4-oxa-2,5-diazaphenanthrenes, compound **3.0** (Figure 1).

1.0 had an IC_{50} of 0.2 μM and is a competitive inhibitor for ATP binding. Kinetic studies indicated that **1.0** has a Ki of ~0.17 μM under a saturated concentration of tau (20 μM) (Figure 1D). It was reported [41] that Cdk5 acts by a random, anticooperative kinetic mechanism. Under such a mechanism, binding of one substrate greatly decreases the affinity for the binding of a second substrate.

2.0 showed competitive inhibition against ATP binding with a Ki of 0.6 μM under a saturated concentration of tau (20 μM) (Figure 1E). The compound also demonstrated noncompetitive inhibition against tau binding under saturating ATP concentration (400 μM) (Figure 1F). Thus, binding of **2.0** to the ATP pocket appears to affect the enzyme binding to a second substrate, tau. The differences in kinetic modes of these two competitive inhibitors to the ATP site may be reflected in their cocrystal structures (see below).

3.0 did not compete with ATP for binding to Cdk5/p25 (data not shown). **3.0** did not inhibit phosphorylation by Cdk5 when tau was used at its Km (~4 μM). At low concentrations of tau (up to 0.6 μM), **3.0** bound competitively with tau with an apparent K_i of 8 μM (Figure 1G) according to a Dixon plot (Figure 1H). The inhibition of **3.0** was abolished at high concentrations of tau. When histone H1 (Km = 80 μM) and a peptide derived from histone H1 (Pro-Lys-Thr-Pro-Lys-Lys-Ala-Lys-Lys-Leu) (Km = 600 μM) were used as substrates at the same low concentrations as tau, **3.0** did not inhibit the phosphorylation of histone H1 and a peptide derived from histone H1 (data not shown). The greater specificity of **3.0** for tau as a Cdk5 substrate was also suggested by comparing the IC_{50}s values of **3.0** for tau (17.0 μM) to FAK (271.8 μM), another well-characterized Cdk5 substrate [42].

Inhibitory Effects in Cells, Toxicity, and Specificity

The effects of the compounds on tau phosphorylation were studied in the neuroblastoma cell line IMR-32 and rat primary neurons. IMR-32 has been shown to contain constitutively active Cdk5 [43]. Cells were incubated with the compounds for 2 hr, lysed, and sequentially analyzed by immunoblot, first with monoclonal PHF-1 antibody, and then with a second polyclonal antibody against total tau (Figure 2A). At 2 hr no toxicity was observed. Total tau was used as a control. **1.0** had a minimal effect on tau phosphorylation in both cell types even at 50 μM, presumably due to low cell permeability. This compound is quite hydrophilic with four hydroxyl groups, which may contribute to the low penetration through the cell membrane. **2.0** had a dose-dependent inhibition on tau phosphorylation in both IMR-32 cells and primary neurons with an EC_{50} < 20 μM. **3.0** inhibited Cdk5/p25 phosphorylation of tau at the PHF-1 sites with an EC_{50} < 50 μM.

Cell viability was assayed in HT1080 cells (Figure 2B). **1.0** had no apparent cytotoxicity up to 100 μM at either 24 or 48 hr incubation. **2.0** had an LD_{50} of 33 μM at 24 and 48 hr incubation. **3.0** had an LD_{50} of 13 μM for 24 hr and 7 μM for 48 hr incubation.

Glycogen synthetase kinase 3β, CDK1, casein kinase 1, protein kinase A, protein kinase C, and Src kinase were tested with these three inhibitors for specificity (see Supplemental Table S1 available with this article online). **1.0** inhibited Cdk5 and CDK1 equally; however, it has a higher IC_{50} toward GSK3β and casein kinase, protein kinase C, and Src kinase. **2.0** is a better inhibitor

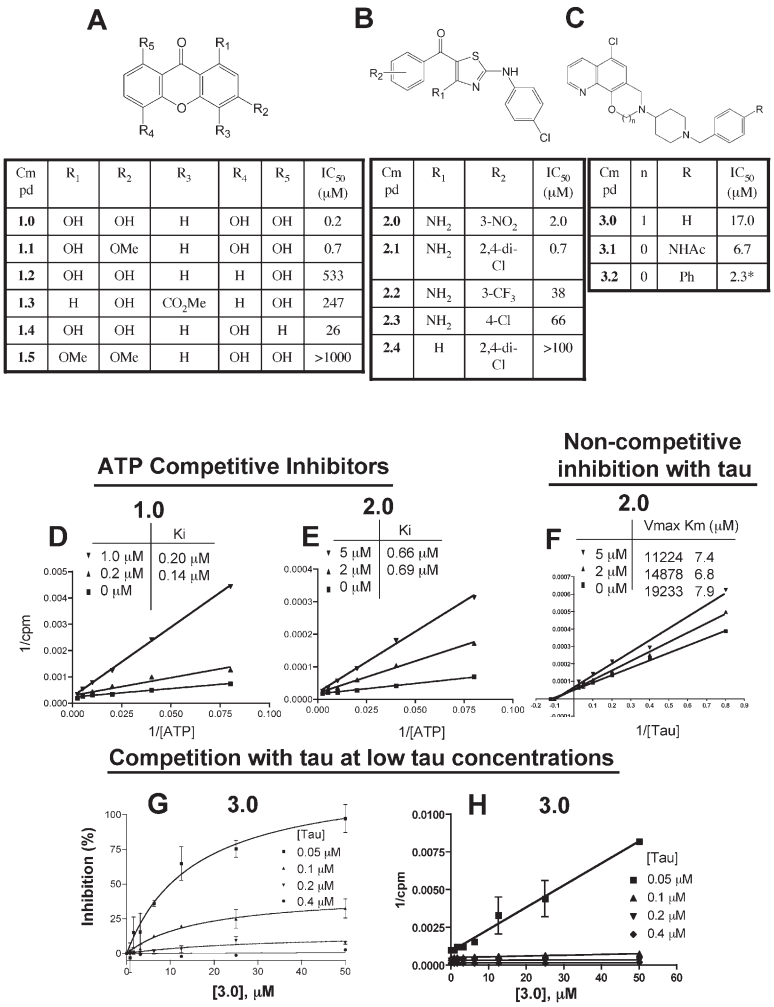

Cmpd	R_1	R_2	R_3	R_4	R_5	IC_{50} (μM)
1.0	OH	OH	H	OH	OH	0.2
1.1	OH	OMe	H	OH	OH	0.7
1.2	OH	OH	H	H	OH	533
1.3	H	OH	CO_2Me	H	OH	247
1.4	OH	OH	H	OH	H	26
1.5	OMe	OMe	H	OH	OH	>1000

Cmpd	R_1	R_2	IC_{50} (μM)
2.0	NH_2	3-NO_2	2.0
2.1	NH_2	2,4-di-Cl	0.7
2.2	NH_2	3-CF_3	38
2.3	NH_2	4-Cl	66
2.4	H	2,4-di-Cl	>100

Cmpd	n	R	IC_{50} (μM)
3.0	1	H	17.0
3.1	0	NHAc	6.7
3.2	0	Ph	2.3*

Figure 1. Chemical Structures, SAR, and Kinetics

(A–C) Chemical structures of Cdk5/p25 inhibitors and structure activity relationships. **3.0** and **3.1** have similar inhibitory properties; however, **3.1** is more soluble. The asterisk indicates that the value for **3.2** is not a true IC_{50} value due to its limited solubility. By curve fitting, we concluded that 50% inhibition was achieved at 2.3 μM.

(D and E) Compounds **1.0** and **2.0** are ATP competitive inhibitors.

(F) Compound **2.0** is also noncompetitive with tau. The degree of phosphorylation by Cdk5 was evaluated by the filter method, as described in Experimental Procedures. Various concentrations of ATP (0–400 μM) for the ATP competition or tau (0–40 μM) for the tau competition were incubated with Cdk5/p25 in the absence (square) or IC_{50} (up triangle) or IC_{80} (down triangle) concentration of inhibitors for 60 min at 30°C. Each point represents mean ± SEM. A graph of the double-reciprocal of the degree of phosphorylation against substrate (ATP or Tau) concentration is plotted.

(G) The inhibition of Cdk5 activity by **3.0** depends on tau concentration. Various concentrations of **3.0** were incubated with four different concentrations of tau as indicated. The degree of tau phosphorylation by Cdk5 was assayed by the filter method as described in Experimental Procedures. The ATP concentration was 400 μM.

(H) Dixon Plot of the inhibitor **3.0**. The reciprocal of Cdk5 activity derived from Figure 3A was plotted against the concentration of inhibitor **3.0** at four different tau concentrations as indicated. Data were analyzed with GraphPad software. Each point represents mean ± SEM.

for GSK3β than Cdk5 and CDK1. It has low activity toward other kinases. **3.0** has 2- to 3-fold greater inhibition toward Cdk5 compared with GSK3β and CDK1 and showed only low activity toward the other kinases.

Cocrystallization of Compound 1.0 with cdk5/p25

To obtain structural information on the mode of binding of **1.0** to Cdk5, we exploited well-diffracting trigonal crystals of the Cdk5/p25 complex [39]. **1.0** was soaked into the crystal, and diffraction data from a frozen crystal were collected to a resolution of 2.1 Å (Supplemental Table S2). The structure was determined using the Molecular Replacement technique (see Experimental Procedures). The structure confirms the kinetic result that **1.0** is an ATP competitor (Figure 3) and also provides an excellent framework to understand the results of the SAR analysis. **1.0** is sandwiched between the hydrophobic ceiling, walls, and floor of the Cdk5 ATP binding site, containing, among others, the side chains of Ile10, Val18, Ala31, Val64, Phe80, Phe82, Leu133, and Ala143. Interestingly, **1.0** forms seven hydrogen bond donor/acceptor interactions with the main chain and side chain atoms of Cdk5, rather than the 3–4 often observed for active site kinase inhibitors. Some of the bonds are suboptimal (see below), suggesting that the compound can be improved to become an even more effective Cdk5 ligand.

Interestingly, **1.0** induces a restructuring of the Gly-rich loop of Cdk5. This occurs via the action of the hydroxyl group at R1, which is involved in two hydrogen bonds with the main chain amide and carbonyl groups of Glu12. We infer from the fact that there is excellent electron density for the Gly-rich loop that these interactions stabilize this loop, which is typically disordered in crystal structures of Cdk5 and other kinases. We observed a single water molecule in the active site of Cdk5 bound to **1.0**. The hydroxyl group at R2 is in proximity to several potential hydrogen bond donors and acceptors, including the amide group of Asp86 and the carbonyl of Ile10. The distances and orientation of these interactions, however, appear suboptimal, suggesting that improved binding affinities may be achieved by appropriate modification of the inhibitor. The hydroxyl group at R4 is within hydrogen bonding distance with the carbonyl group of Glu81 (2.7 Å) and the main chain amide of Cys83 (2.9 Å). These interactions explain why removal of the hydroxyl from this position results in loss of activity. In other Cdk5-inhibitor com-

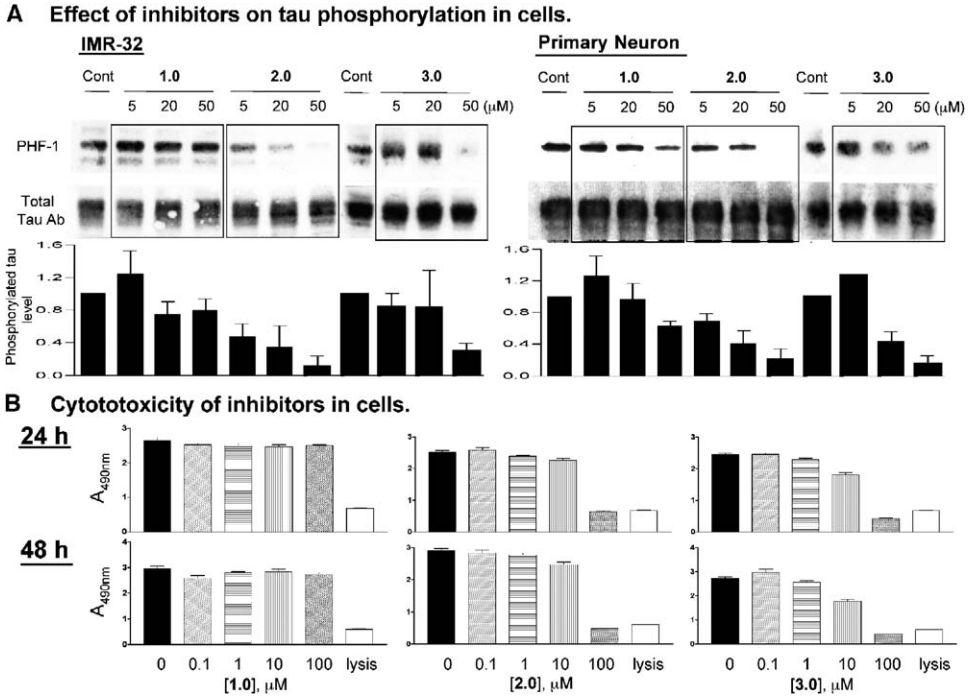

Figure 2. Cell-Based Assays

(A) Effect of inhibitors on tau phosphorylation in cells. Three different concentrations of inhibitors were incubated in culture medium with IMR-32 cells or primary neuron for 2 hr at 37°C. After incubation, cells were lysed and Western blot analysis were followed using PHF-1 or total tau antibody. Upper blots are representative of three separate experiments and lower bar graph shows relative band intensity (mean ± SEM). (B) Cytotoxicity test of inhibitors. Various concentrations (0.1–100 μM) of inhibitors were applied into HT1080 cells and incubated for 24 or 48 hr. After incubation, cells were lysed and cell titer reagent (CellTiter 96 Aqueous One Solution Cell Proliferation Assay-Promega) were added followed by incubation at 37°C for 2 hr. Color intensity was measured at 495 nm.

plexes, including those with roscovitine, indirubin, aloisine [39], and **2.0** (see below), the carbonyl group of Cys83 engages in a hydrogen bond with the inhibitor. In the complex with **1.0**, no suitably placed groups in the inhibitor can engage the carbonyl oxygen of Cys83. Finally, the hydroxyl group at R5 is hydrogen bonded with the side chain of Asn144, which replaces the catalytic Asp144 in the inactive version of Cdk5 used for crystallization. We expect that a similar interaction is formed with Asp144, explaining why the removal of this substituent decreases the potency of the compound. In summary, the structure points at the R1, R4, and R5 hydroxyl groups as being most critical for binding, in agreement with the SAR analysis (see below).

Cocrystallization of Compound 2.0 with cdk5/p25

We also determined the 1.95 Å crystal structure of **2.0** bound to the Cdk5/p25 complex using essentially the same strategy described above (Figure 3). The electron density is usually significantly weaker for one of the two Cdk5/p25 complexes present in the asymmetric unit of the trigonal and well-diffracting crystal form of Cdk5/p25 used for these experiments, and we usually limit our analysis to the better defined of the two complexes. In the particular case of **2.0**, however, electron density for the inhibitor was only observable in the active site of the less-defined Cdk5-p25 complex, while no density was present in the other complex. This might reflect the fact that the penetration of the compound into the active site of Cdk5 imposes a conformational change that is more easily sampled in the crystals by the more mobile (and therefore disordered) complex. At any rate, the electron density of the inhibitor and of the surrounding protein moiety was perfectly suited for unambiguous interpretation of the orientation of **2.0**. As with **1.0**, we found that the inhibitor occupied the ATP binding pocket of the kinase. Like most ATP-site kinase inhibitors, **2.0** formed three hydrogen bonds with the main chain atoms of Glu81 and Cys83. A fourth hydrogen bond involved the nitrobenzene moiety of **2.0** and engages the ϵ amino group of Lys33. There is no comparable ordering of the Gly-rich loop to that observed in the complex with **1.0**. As a consequence, this loop (residues 11–15) is partly disordered and was not modeled. The interaction of **2.0** is partly reminiscent of the mechanism of binding of roscovitine to Cdk5 [39]. In particular, the central 5-atom system and the 4-chloroaniline ring of **2.0** are positioned in the active site of Cdk5, like the 5-atom ring of purine and the benzylamine substituent in roscovitine, respectively. No equivalent of the interaction of the nitrobenzene group in **2.0** with Lys33 is present in the roscovitine complex, however.

Modeling of the **2.0** cocrystal as an aligned overlay with four other Cdk5 inhibitor structures (**1.0**, aloisine-A, indirubin-3′-ozime, and (R)-roscovitine) revealed a sig-

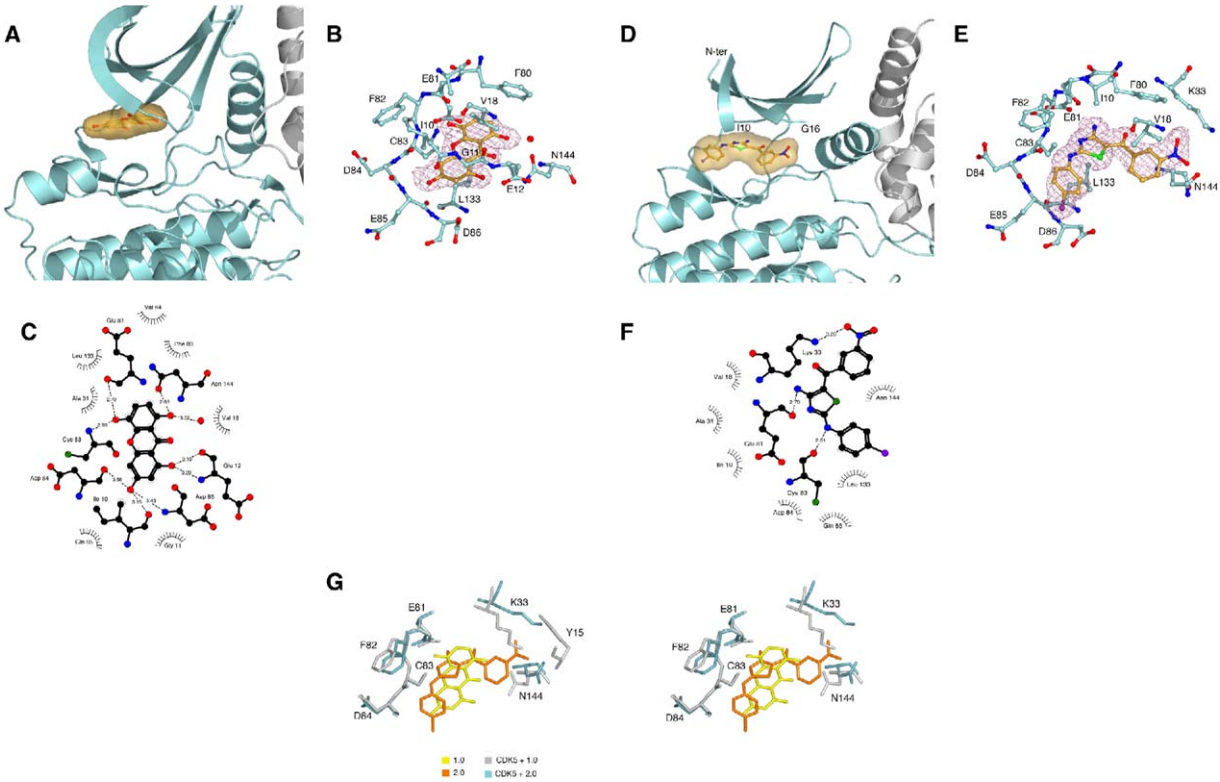

Figure 3. Crystal Structure of **1.0** and **2.0** Bound to Cdk5/p25

(A and D) Ribbon model of Cdk5/p25 (light blue and gray) in complex with the inhibitor (space-filling model).

(B and E) Close-ups of the catalytic site of the kinase complexed with inhibitors. The residues of Cdk5 that contact the bound ligand are depicted in ball-and-sticks, carbon atoms are in gray (protein) and tallow (inhibitor), oxygen atoms in red, and nitrogens in blue. Electron density is shown in pink for the inhibitor only (contoured at 3 sigma level).

(C and F) Schematic drawing of the interaction between Cdk5 and inhibitors. Residues forming van der Waals interactions are indicated as dashed moons, those engaged in hydrogen bonds are shown in ball-and-stick representation. Hydrogen bonds are depicted as dotted lines with the donor-acceptor distance given in angstroms.

(G) Structural superposition of the active site of Cdk5 with the two ligands.

nificant movement in two side chains (Asn144 and Lys33) due to the **2.0** nitrophenyl group (Figure 4). Wild-type Cdk5 has an aspartate in position 144, instead of an asparagine in the inactive mutant. Therefore, Asn144 was computationally mutated to an aspartate (see Experimental Procedures). In the aligned mutated and minimized structures, the position of Asp144 in the **2.0** structure is not as distinct from its positions in the other structures, but the position of Lys33 is still unique (Figure 4). This observation fits well with the kinetic data that **2.0** is a noncompetitive inhibitor of tau, and perhaps this change in the side chain conformation plays some role in the mode of tau inhibition.

Structure Activity Relationship of cdk5/p25 Inhibitor

Several derivatives of bellidin (compound **1**) were assayed for Cdk5/p25 inhibitory activity. Bellidifodin, **1.1**, a methylated derivative of bellidin, had comparable inhibitory activity with an IC_{50} = 0.7 μM (Figure 1). This example demonstrated that the hydroxyl group at the 3-position of the xanthen-9-one ring in bellidin was not necessary for Cdk5/p25 inhibitory activity. However, the natural product norsterigmatocystin, **1.2**, was practically devoid of Cdk5/p25 inhibitory activity with an IC_{50} = 533 μM. This example illustrated that the hydroxyl group at the 4-position of the xanthen-9-one in bellidin was essential for Cdk5/p25 inhibitory activity. The xanthen-9-one derivative **1.4**, which lacks the hydroxyl group in the 8-position, had diminished activity (IC_{50} = 26 μM) compared to **1.0**. However, when the hydroxyl group is methylated as in **1.5**, all Cdk5/p25 inhibitory activity was lost (IC_{50} > 1000 μM).

These conclusions were supported by an X-ray analysis of a cocrystal of Cdk5/p25 and bellidin. The SAR results were analyzed through a comparison between actual and optimized ligand charge distributions. The latter identifies and corrects points of electrostatic noncomplementarity (Figure 5A). In the right panel, red (blue) indicates atoms whose partial atomic charge is more negative (positive) than optimal; atoms drawn with larger radii have a more substantial effect on the binding affinity than do those with smaller radii. Atoms near group A have a small computed effect on affinity due to their large solvent exposure, while those near groups B and C have a large effect due to being buried in the pocket. Many charge-sensitive regions of **1.0** are

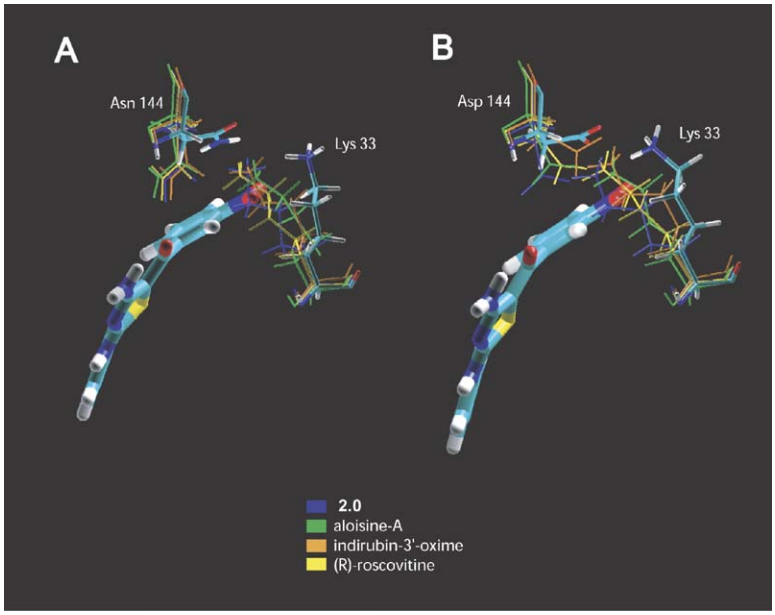

Figure 4. Displacement of Amino Acid Side Chains by **2.0**

(A) Aligned overlay of Cdk5 Asn144 and Lys33 from five Cdk5/inhibitor structures with **2.0**. The amino acids from the Cdk5/**2.0** structure, as well as **2.0**, are shown in atom colors, while amino acids from the other structures are colored according to the legend. Note the significant movement in these two side chains due to the **2.0** nitrophenyl group. Wild-type Cdk5 has an aspartate at position 144 instead of an asparagine in the kinase-dead mutant. As a check, Asn144 was computationally mutated to an aspartate. (B) Aligned mutated and minimized structures (the minimization included both side chains in the mobile region). Note that the position of Asp144 in the **2.0** structure is not as distinct from its positions in the other structures, but the position of Lys33 is still unique.

already close to charge optimized, i.e., not many large spheres are highly colored.

Several derivatives of **2.0** were also assayed for Cdk5/p25 inhibitory activity (Figure 1). Changing the aryl ketone substituents was tolerated in the case of **2.1** (IC_{50} = 1.4 μM). However, other aryl ketones, such as **2.2** and **2.3**, were detrimental to activity. Finally, removal of the amino group on the central thiazole ring (i.e., **2.4**) resulted in loss of all Cdk5/p25 kinase inhibitory activity. This observation was supported by the Cdk5/p25 and **2.0** cocrystal structures that showed the participation of this amino group in an H-bond, and is therefore expected to be critical for binding.

A similar charge-optimization analysis for **2.0** is shown (Figure 5B). Atoms interacting with Cys83 and Glu81 are near optimal, though there is room for improvement in the group that interacts with Glu81:O; the nitrogen appears to be too negative. Interestingly, based on an alignment of Cdk5 with Cdk2/ATP complex, **2.0** and ATP share two interactions—H bonds with residues 81 and 83—while **2.0** has a third interaction with the carbonyl of Cys83.

Defining the Chemical Space within the Cdk5 ATP Pocket

Recently, the crystal structures of the active CDK5/p25 kinase complexed with three inhibitors (R)-roscovitine, aloisine-A, and indirubin-3′-oxime were reported [39]. These compounds are ATP-antagonists binding into the well-conserved catalytic pocket of the kinase with IC_{50} values in the range of 0.1–0.2 μM. When these three compounds plus the two compounds presented here are aligned, they all share overlapping chemical space (Figure 6A). All five inhibitors interacted with the N-H group of Cys83, four with the carbonyl group of Cys83, and three with the carbonyl group of Glu81 (Figure 6A). To look for common features among the five inhibitors, the actual partial atomic charge values of all five inhibitors were compared to their charge-optimized values (Figure 6B). The critical interactions with Cdk5, Glu81, and Cys83 as a whole seem to be well optimized in all five inhibitors. By fitting all of the inhibitors into their van der Waals volume, it is apparent that in one dimension they share a relatively flat plane (Figures 6C and 6D). The hydrophobic contacts are generally made above and below the flat binding pocket, while polar interactions are made along the flat dimension of the inhibitors (Figure 6E).

When each of the five inhibitors was aligned inside a representation of its corresponding Cdk5 ATP binding site, a potential pocket is present in all five structures (Figure 7). This pocket contacts Cdk5 residues Leu55, Val64, Phe80, Asn144, Phe145, and Ala143 and represents a potential space for rational drug design.

Discussion

The three compounds reported here inhibit Cdk5 by distinct mechanisms and each suggests strategies for future inhibitor optimization. In the case of **1.0**, both the kinetic and crystallographic data demonstrate that the compound binds competitively with ATP in the ATP pocket. The highly conserved nature of this binding pocket presents a challenge for the design of specific inhibitor compounds. Comparisons with other compounds that bind to the same site suggest that molecules containing fused aromatic or heterocyclic rings bind to the ATP site by fitting into the planar groove. Based on an alignment of Cdk5 with Cdk2/ATP, this groove is probably the site occupied by the adenine when ATP binds. The very strong skew toward compounds with this planar configuration may be due to a characteristic of this binding pocket or limitations in the diversity of the chemical library. However, portions of some inhibitors, such as the nitrophenyl ring of **2.0** or the phenyl ring of roscovitine, extend uniquely into

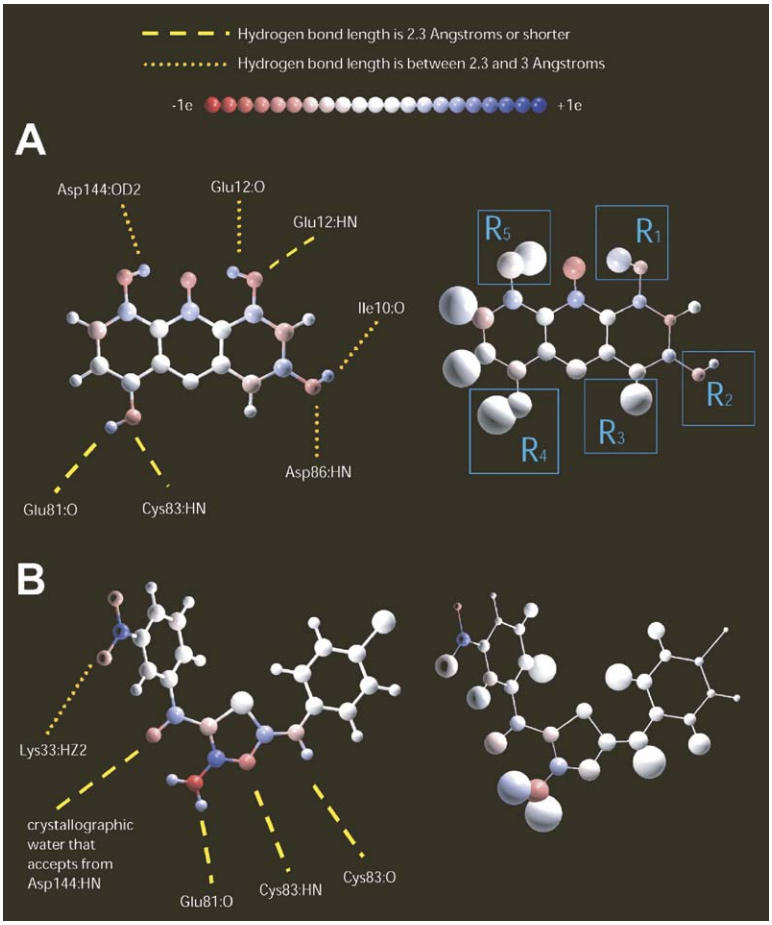

Figure 5. Charge Optimization

(A) At left, the actual partial atomic charge values of **1.0**, as well as a schematic of hydrogen bonding interactions. At right, the color on each atom represents the difference between its actual partial atomic charge and the charge-optimized value. A white atom indicates that the atom's current charge is very close to the optimum. The radius of each atom is proportional to the magnitude of the diagonal element of the ligand desolvation matrix corresponding to that atom, which correlates with the sensitivity of the molecule's binding energy to the charge on that atom. A large atom in the figure, therefore, indicates that the molecule's binding energy is very sensitive to that atom's charge. As the charges on the surrounding residues are critical to the electrostatic interactions, the computationally mutated N144D Cdk5 structures were used and the surrounding residues were minimized along with it.

Group R_2: **1.0** was experimentally compared to an analogous molecule where the O-H group indicated by "R_2" was methylated, and the IC_{50} did not change considerably (0.2–0.7 μM). Note that this group is neither well optimized nor in a location where the binding energy is sensitive to its charges.

Group R_4: **1.0** was experimentally compared to an analog that lacked the O-H group indicated by "R_4," and the IC_{50} became worse by a factor of >1000 (0.2–532.7 μM). Note that this group is both well optimized and in a location where the binding energy is sensitive to its charges. Also, this group is involved in making the interactions with Cys83 and Glu81 that have been highly conserved in Cdk1, 2, 5, and 9 inhibitors, and other kinase inhibitors.

Group R_5: **1.0** was experimentally compared to an analog that lacked the O-H group indicated by "R_5," and the IC_{50} became considerably worse (0.2–25.5 μM), though not as strongly as the effect of deleting R_4. This intermediate effect can be rationalized by noting that although the binding free energy is expected to be quite sensitive to the charges on this group and the group itself is relatively well optimized, the surrounding charges are not near optimal, as measured by the charges' closeness to the corresponding charges on the charge-optimized molecule.

Group R_1: **1.0** was experimentally compared to an analog in which the –OH groups indicated by R_1 and R_2 were both methylated and the IC_{50}'s differ enormously (0.2 and >1000 μM). The perturbation to R_1 alone is expected to have a small effect electrostatically. The observed effect is somewhat larger and may be due to cooperative effects with group R_2, such as through an altered binding conformation/tautomer.

(B) Results from charge optimization on the **2.0** inhibitor are shown analogously to those in (A). Note that the charges on the atoms interacting with Cys83 are nearly optimal, while the nitrogen atom in the NH2 interacting with Glu81 is too negative. Based on alignment with Cdk2/ATP complex, ATP appears to make two H bonds with residues 81 and 83, while **2.0** has a third interaction with the carbonyl of Cys83. No such interaction is seen for ATP. These three interactions are the same ones that ATP may make with Cdk5, based on an alignment of Cdk5 with a Cdk2/ATP complex. An explanation of SAR data is not attempted based on charge optimization data because much of the SAR changes were made on the nitro ring, which was very close to the unmodeled glycine-rich loop.

areas of the ATP pocket not occupied by any of the other.

2.0 is also a competitive inhibitor for ATP but a noncompetitive inhibitor for tau. As such, binding of the compound to the ATP pocket affects tau binding. Noncompetitive inhibitors decrease maximum catalytic activity (V_{max} or B_{max}) with minimal effect on substrate binding affinity (K_m or K_d). A possible basis for this effect may be apparent in the cocrystal, which revealed a rotational movement of two side chains (Asn144 and Lys33) due to the nitrophenyl group of **2.0**. Interestingly, none of the other compounds show this movement, nor do the other inhibitors demonstrate this kinetic profile.

3.0 does not compete with ATP but does compete with tau at low tau concentrations. Given the complexity of tau phosphorylation [44], inhibitors could be expected with unusual kinetic profiles. In this case, **3.0** may interfere with tau binding to the enzyme. The modest specificity of the compound for Cdk5 supports this possibility; however, more definitive data from attempted cocrystallization failed to detect any density corresponding to the inhibitor. However, Cdk5-p25 crystals soaked with **3.1**, an active derivative of **3.0**, showed a rearrangement of the activation loop at position Val163. The structure of Cdk5-p25 revealed a peculiar orientation of the V162 carbonyl, very similar to what was observed in fully active Cdk2-cyclinA phosphorylated on T160, despite the fact that the T-loop of

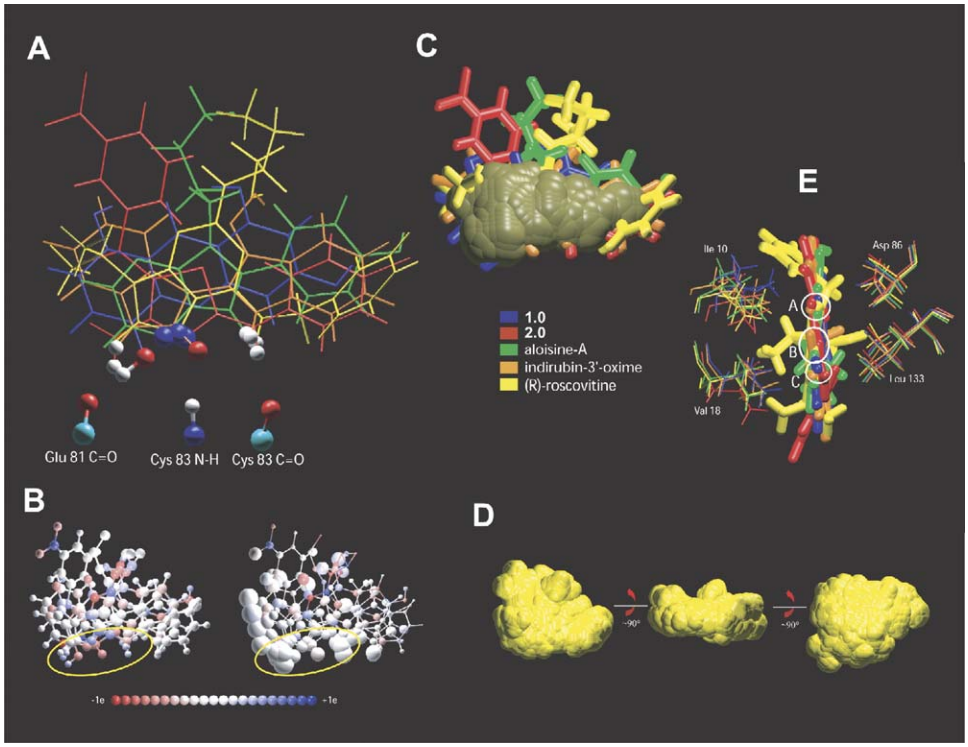

Figure 6. Comparison of Several CDK5 Inhibitors

(A) Aligned overlay of the five inhibitors. Inhibitor atoms that are involved in making hydrogen bonds to Glu81 or Cys83 are shown as spheres, as are the relevant atoms in Glu81 and Cys83. Oxygen, nitrogen, hydrogen, and carbon atoms are colored red, blue, white, and cyan, respectively. Note that all five inhibitors interact with the N-H group of Cys83, four with the carbonyl group of Cys83, and three with the carbonyl group of Glu81.

(B) Aligned overlays of the five inhibitors. At left, the atoms are colored according to their partial atomic charges, and at right, they are colored red (blue) if their charge is more negative (positive) than their optimal charges. The circled region shows the atoms that interact with Glu81 and Cys83 of Cdk5. Note that their charges are quite close to the corresponding charges in the charge-optimized molecules, and the binding energies to Cdk5 are sensitive to the charges of these atoms. This analysis uses charge-optimization theory to highlight the importance of satisfying these interactions. Computationally mutated N144D Cdk5 structures were used in all five charge optimizations.

(C) Aligned overlay of the five inhibitors in which the gold volume represents van der Waals volume that is common to all five inhibitors. Note that the five inhibitors share a common plane.

(D) Different views of the union volume of the aligned five inhibitors, i.e., the volume occupied by at least one of the inhibitors. Note that the shape is relatively flat in one dimension.

(E) Aligned overlay of the five inhibitors, colored according to the key above. The Cdk5-aligned residues shown are "critical contact residues," defined by having their solvent-accessible surface area change by at least 10 $Å^2$ upon binding to each of the five inhibitors. The regions A, B, and C denote the general locations of atoms involved in forming hydrogen bonds with Cys83 H, Cys83 O, and Glu81 O, respectively. Note that the hydrophobic contacts are generally made above and below the flat binding pocket, while polar interactions are made along the flat dimension of the inhibitors.

Cdk5 is not phosphorylated [23]. The interpretation given was that Cdk5 does not need to be phosphorylated on S159 and full activation is brought about by the mere binding of p25/p35. This fully active conformation of the T-loop is unchanged in all the Cdk5-p25 structures observed with the other cocrystals (more than ten structures). However, when soaked with **3.1**, the T-loop assumed a different conformation, in which the V162 carbonyl adopts an orientation resembling the one observed in unphosphorylated Cdk2-cyclin A (and hence not fully active). This conformation may explain the mechanism underlying the inhibition kinetics, particularly if the inhibitor is bound with a very low occupancy.

In conclusion, this report suggests strategies to discover specific Cdk5 small molecule inhibitors. Unique features of the Cdk5 ATP binding may permit selective binding of ATP competitors. On the other hand, small molecules that bind outside the Cdk5 ATP pocket, an example of which is suggested by compound **3.0**, present opportunities for selective inhibition.

Significance

Cdk5 is an attractive target for a diverse set of medical conditions that affect the nervous system and for which no treatments currently exist. Nearly all small molecule inhibitors discovered to date compete with ATP and are likely to bind to the ATP pocket. The conservation of the ATP binding pocket among Cdk5-related kinases represents a challenge to the discovery of more selective compounds. We describe three

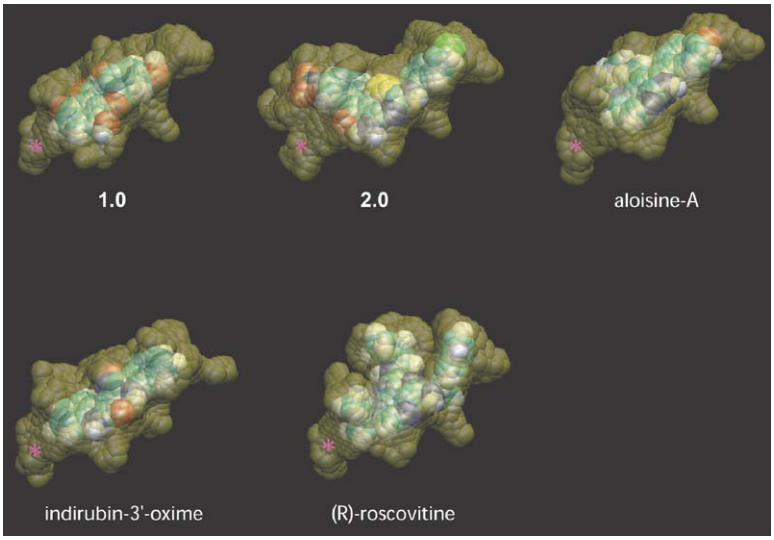

Figure 7. Binding Pocket Representations

Each of the five inhibitors aligned inside a representation of its corresponding Cdk5 structure's ATP binding site. The opening to solvent is the bulge on the upper right of each representation. The pink asterisks represent a potential pocket present in all five structures into which one might rationally design in the future work; this pocket contacts CDK5 residues Leu55, Val64, Phe80, Asn144, Phe145, and Ala143. (Note: for **2.0**, Aloisine-A, and indirubin-3′-oxime, there is missing density in the crystal structure in a small region above the inhibitors as viewed in the figures, and as a result, the ATP binding site appears larger in this region than it might actually be.)

novel Cdk5 inhibitors, each with a distinct mode of binding, and a computational analysis of how five different inhibitors fit into the Cdk5 binding pocket. One compound pushes residues aside to make room for the entry of a nitrophenyl group into the ATP pocket. The SAR and charge optimization analysis maps out the importance of filling and properly charging up different regions of the binding pocket. Results such as the identification of a cavity within the ATP binding pocket that was unfilled by all five inhibitors represents a direction for rationale design of novel compounds. Finally, one the compounds offers the first suggestion that small molecule inhibitors of Cdk5, which are noncompetitive with ATP, might be discoverable.

Experimental Procedures

Preparation of Human Recombinant Tau

Tau was prepared according to the method previously described [40]. Briefly, a plasmid with the longest human tau cDNA was transformed into BL21 competent cells, following a procedure described in Novagen's pET system manual. After induction of the protein expression using IPTG, cell pellets were collected and resuspended with MOPS buffer. The cell suspension was lysed by Microfluidizer (Technika, Chester, CT). Taking advantage of the heat stability of tau [45], tau was placed in a boiling water bath for 10 min and protein aggregates were removed by centrifugation. The recombinant tau was further purified by passing the diluted supernatant over a MonoS HiTrap column overnight. The protein concentration was measured by the BCA method using bovine serum albumin as the standard, and tau was stored at −80°C until used.

Synthesis of Compound Derivatives

See Supplemental Data.

In Vitro Kinase Assay of Tau Phosphorylation

Cdk5, ^{33}P-ATP, and cofactors were added in the presence of tau protein. The reaction mixture was incubated to allow Cdk5 to transfer ^{33}P from ATP to tau. After transferring the mixture to a Durapore PVDF membrane (Millipore), trichloroacetic acid (Sigma) was added to stop the reaction and precipitate proteins. The filters were washed to remove the unreacted components. Then, the filter was punched and the radioactivity of the precipitate bound on the filter was counted. To test the inhibitory effects of the compounds, tau, histone H1, and a peptide derived from histone H1 (Pro-Lys-Thr-Pro-Lys-Lys-Ala-Lys-Lys-Leu) were used as substrates to measure the Km for each substrate (data not shown).

Phosphorylation of Tau in ELISA Format

Concentrated Sulfo-NHS-LC-LC-Biotin (Pierce) was added to tau (2 mg/ml) at a 20-fold molar excess. The reaction mixture was placed on ice for 3 hr. Excess biotin reagent was removed by Centricon (Millipore) in the presence of a large volume of phosphate-buffered saline. Biotinylated-tau was stored at −80°C until use.

The assay conditions for phosphorylation of biotinylated tau were similar to those described in the filter assay without the [^{33}P]ATP. The reaction was carried out for 60 min at 30°C and terminated by addition of 10 μl of 50 mM EDTA to a final concentration of 10 mM. 40 μl of the reaction mixture was transferred to a 384-well plate coated with streptavidin (Greiner). The plate was incubated at room temperature for an additional 1 hr to allow for capture of the biotinylated tau. The unbound tau was removed by six washes with 120 μl of PBST each. PHF-1 was used as a primary antibody, and a rabbit anti-mouse antibody, which was conjugated with horseradish peroxidase (Promega), was used as a reporter. 3, 3′,5,5′-Tetramethyl benzidine (TMB) was added as a substrate for the peroxidase to develop the color product according to the manufacturer's instruction (PharMingen). The color was quantified using a plate reader (SpectraMaxx 384, Molecular Devices) at 450 nm.

Kinetic Studies

Kinase assays were performed with various concentrations of ATP or tau with cdk5/p25. The data were analyzed by a nonlinear least-squares program to determine kinetic parameters using GraphPad software.

Crystallography

Protein expression and purification were performed as previously reported [23]. Crystallization of the complex was carried out by the hanging-drop vapor diffusion technique using the streak-seeding method for crystal optimization. Crystals were harvested into a stabilizing solution of 13% (w/v) PEG 3350, 100 mM KI, 100 mM bisTris-Propane (pH 7), and 10 mM DTT supplemented with 1 ml of 10 to 100 mM inhibitor molecule previously dissolved in DMSO. Soaks were carried out for 48–72 hr, and crystals were subsequently cryoprotected by step-wise addition of stabilizing solution plus 50% (w/v) glycerol up to a final concentration of 20% glycerol before freezing in liquid nitrogen. Data were collected at beamlines ID14-1 and ID14-2 of the European Synchrotron Radiation Facility

(ESRF) on an ADSC Q4R detector (λ = 0.933 Å). Data processing and reduction were carried out with the HKL package [46]. Details of the data collection and reduction are reported in Supplemental Table S2. The structure was determined by molecular replacement with the atomic coordinates of the Cdk5-p25 complex (Protein Data Bank code 1H4L) as the search model utilizing the program AMoRe [47]. After the first cycles of rigid-body refinement, difference Fourier maps displayed clear electron densities in the active site for the inhibitors. At this stage, a run of 15 cycles of ARP/wARP [48] was performed to improve the density in the active site without model bias. The resulting density was used to manually fit the inhibitor models whose geometry was generated with the DRG program [49]. Subsequent refinement was pursued with alternating cycles of interactive model building and CNS [50] or REFMAC [51] program suites. Bulk solvent correction and anisotropic B factor scaling were applied throughout the refinement procedures. Toward the end of the refinement, water molecule positions were added using the water-pick routine included in CNS. TLS refinement was implemented at the end of the refinement protocol to separately model the anisotropic movement of the N- and C-terminal lobes of Cdk5 and of p25. The electron density map is significantly weaker for one of the two Cdk5-p25 complexes contained in the a.s.u., and most of the analyses reported here rely on the better ordered one. The final model of the complex with compound **1.0** consists of residues 1–292 for cdk5 and 145–293 for p25. Final refinement statistics are reported in Supplemental Table S2.

Cytotoxicity Test

HT 1080 cells were prepared in clear Nunc 384-well tissue culture plate at 5000 cells per well in a 45 μl volume. Various concentrations (0.1, 1, 10, and 100 μM) of compounds were added and then incubated for 24 or 48 hr (one plate for each time point). 10 μl of cell titre reagent (CellTiter 96 Aqueous One Solution Cell proliferation Assay-Promega) was added to each well. After incubation, cells were lysed with 2 μl lysis buffer (9% triton) and incubated at 37°C for 2 hr, and color density was measured at 495 nm.

Cell Culture and cdk5 Kinase Activity Assay in Cells

Inhibitors were incubated with human neuroblastoma IMR-32 cells or primary neurons from rat brain for 2 hr at 37°C. We used IMR-32 cell line because it was reported that cdk5 is active in the cells [43]. The regulatory subunit of cdk5, p35 is constitutively expressed in IMR-32 cells. The cell line was maintained under subconfluent conditions in EMEM medium (ATCC), supplemented with 0.5% nonessential aminoacids, penicillin (100 U/ml), streptomycin (100 μg/ml), glutamine (2 mM), and 10% (v/v) fetal bovine serum in 75 cm^2 tissue culture flasks at 37°C in a humidified atmosphere with 5% CO_2. The growth medium was changed twice a week.

Cell extracts were obtained by lysing cells in lysis buffer (50 mM Tris-HCl [pH 7.5], 250 mM NaCl, 5 mM EDTA [pH 8.0], 0.1% NP-40, 5 mM DTT) supplemented with protease inhibitors (Roche) for 30 min at 4°C. Cell lysates were recovered and centrifuged at 10,000 × g for 5 min at 4°C. Protein concentration was determined by bicinchoninic acid (BCA) assay (Pierce).

Western Blot and Antibodies

Equal amounts of total protein were size fractionated by SDS-PAGE (10% Tris-Glycine gel, Invitrogen) and transferred to a nitrocellulose membrane (Midwest Scientific). After blocking nonspecific binding by incubation overnight at 4°C with phosphate-buffered saline (GIBCO) containing 0.01% Tween 20 (PBST) and 5% nonfat milk, membranes were washed in PBST. For a determination of the level of total and phosphorylated tau, membranes were incubated for 1 hr at RT with rabbit polyclonal anti-human tau (1:1000) and PHF-1 antibody, respectively. After incubation with the secondary antibody for 1 hr, membranes were washed with PBST. Then, membranes were incubated with chemiluminescence dye (New England Biolabs) for 1 min at room temperature and exposed to X-ray film (Kodak).

Anti-human tau antibody was purchased from Biosource (Camarillo, CA). A phosphorylation-dependent anti-tau antibody (PHF-1) was a generous gift from Dr. Peter Davies (Albert Einstein College of Medicine, New York).

Computational Methods

Molecular Models

All crystal structures were systematically prepared for computational analysis using prepublication versions of the crystallographic coordinates. The amide groups of Asn and Gln residues and the imidazole rings of His residues were flipped as necessary by examining the local side chain environments, and the tautomer/protonation state of each histidine was also determined by visual inspection. Crystallographic water molecules that made fewer than two hydrogen bond contacts with protein atoms within 3.5 Å were eliminated, as well as those with a thermal B factor greater than 50. The HBUILD facility [52] in the CHARMM software package [53] was used to build all hydrogen atom positions. The CHARMm22 parameter set [54] was used for all protein atoms, with the TIP3P water model. Appropriate CHARMm22 atom types were assigned to each ligand molecule. Partial atomic charges for each ligand were obtained from ab initio quantum mechanical calculations, by first using the GAUSSIAN98 package [55] with the restricted Hartree-Fock SCF approach and the 6-31G* basis set for geometry optimization starting from the ligand crystallographic coordinates. Then, a restrained fitting to the electrostatic potential (RESP) [56] was performed to determine the partial atomic charges [57].

Alignment of Structures

Alignment of all five CDK5/p25/inhibitor structures was done using the MULTI facility in the program ProFit (Andrew C.R. Martin, http://www.bioinf.org.uk/software/profit/; [58]), which minimizes the rmsd of a structure to the average of the other structures until convergence is reached. The atoms involved in the alignment were α carbons of residues within 5 Å of all five inhibitors in their respective structures. Using a 7 Å cutoff did not change the alignment noticeably.

Common and Union Volumes

The intersection and union volumes of the five inhibitors were determined by laying a 0.25 Å cubic grid over the aligned overlay of inhibitors and placing 1 Å radius spheres at grid points if the entire sphere was inside all five inhibitor volumes (for the common volume) or at least one inhibitor's volume (for the union volume). CHARMm22 vdW radii were used for the generation of the inhibitor volumes.

Solvent-Accessible Surface Area Calculations

The critical contact residues were defined by having their solvent-accessible surface area (SASA) change by at least 10 $Å^2$ upon binding. SASAs of the receptor residue atoms were calculated analytically using the CHARMM software package and CHARMm22 van der Waals radii. A probe radius of 1.4 Å was used.

Charge Optimization

The partial atomic charges of each ligand were adjusted to optimize its binding affinity to Cdk5/p25 in continuum solvent according to theory [59–61]. Because one goal in this study was to compare the optimization data with SAR results on kinase-active Cdk5, Asn144 in each crystal structure was computationally mutated back to wild-type aspartate. This was done in two ways to check the robustness of the results. In the first method, the Asp was placed in the exact conformation that had been occupied by the Asn. In the second method, Asp144 and all residues and water molecules with a side chain heavy atom or polar hydrogen within 3 Å of side chain 144 were allowed to minimize. The rest of the protein, including the entire protein backbone, and the inhibitor and water molecules were kept fixed. Minimizations were carried out using the adapted-basis Newton-Raphson functionality (developed by D.J. States; see [62]) in CHARMM. Methods 1 and 2 produced qualitatively similar results. As a control, each inhibitor was also allowed to minimize in separate runs, and in each case, the minimized structure did not vary significantly from the unminimized structure, and results generated were qualitatively similar. In this paper, all N144D results were obtained using method 2, where the structures have been minimized.

Matrix elements for the desolvation and interaction of ligand charge centers upon binding to Cdk5/p25 were calculated by solving the linearized Poisson-Boltzmann equation with iterative finite-

difference methods using a locally modified version of the DELPHI software package [63–65]. A 129 × 129 × 129 cubic grid was used, corresponding to approximately 3.3 grid units/Å for these complexes. A previously published focusing and translating procedure was used [66]. The external dielectric constant was 80 and the protein dielectric constant was 4. PARSE radii [67] were used, and hydrogens were included only on aromatic and polar groups. The solvent probe radius used to determine the molecular surface was 1.4 Å and the Stern layer distance was set to 2.0 Å with a salt concentration of 0.145 M. From solving the potentials in the bound and unbound states by charging each ligand atom center to +1.0e, ligand desolvation matrices and interaction vectors used in the charge optimization process were assembled. The actual unconstrained charge optimizations were done using locally written software [68]. Constrained optimizations were also performed using the LOQO software package [69, 70], where the total charge was constrained to be integral or where certain charges were held fixed.

ATP Binding Site Definition

The shapes of the ATP binding pocket in the various complexes were defined using an iterative method that, at each iteration, placed new spheres at user-defined points inside the pocket and minimized the energy of all existing spheres while keeping protein atoms fixed. During a minimization, only van der Waals (vdW) interactions were included in the energy calculation, so that spheres would move as close to protein and to each other as possible, "filling up" the active site. Then, at the subsequent iteration, new spheres were again placed at the same, fixed user-defined points and the vdW energy was again minimized, allowing all spheres present to move. Minimization was done with CHARMM, using CHARMm22 parameters for the protein atoms. Water and inhibitors were removed from the structure, leaving only protein. The vdW well depth of a sphere-sphere interaction was set at 0.1 kcal/mol, and the distance of maximal vdW interaction was fixed at 0.6 Å. The optimal sphere-protein atom distance was set to (1.0 Å + the vdW radius of the protein atom). 100 steps were taken at each minimization. As the binding pockets for the various complexes differed in size, the total number of iterations for each pocket was chosen so that the entire binding pocket was full and spheres were "spilling" out of the pocket. The radius of the spheres for visualization purposes was 1.0 Å.

Visualization Software

All images were visualized using the program VMD [71]. Certain figures in this paper were generated using the Raster3D package [72].

Supplemental Data

Supplemental Data include two tables and Supplemental Experimental Procedures and can be found with this article online at http://www.chembiol.com/cgi/content/full/12/7/811/DC1/.

Acknowledgments

We thank John Lew, Li-Huei Tsai, and Ross Stein for their comments and Michael Altman for insightful discussions and for scripts to generate the ATP binding site shapes as well as the common and union volumes of the inhibitors. We also thank Min Liu and Ken Auerbarch for their technical help. This work was partially supported by NIH grants (GM065418 to B.T. and NS45327 to K.S.K.), the Institute for the Study of Aging, and the Department of Energy Computational Science Graduate Fellowship (DE-FG02-97ER25308 to M.L.R.).

Received: February 13, 2005
Revised: April 13, 2005
Accepted: May 11, 2005
Published: July 22, 2005

References

1. Mapelli, M., and Musacchio, A. (2003). The structural perspective on CDK5. Neurosignals *12*, 164–172.
2. Cruz, J.C., and Tsai, L.H. (2004). A Jekyll and Hyde kinase: roles for Cdk5 in brain development and disease. Curr. Opin. Neurobiol. *14*, 390–394.
3. Hellmich, M.R., Pant, H.C., Wada, E., and Battey, J.F. (1992). Neuronal cdc2-like kinase: a cdc2-related protein kinase with predominantly neuronal expression. Proc. Natl. Acad. Sci. USA *89*, 10867–10871.
4. Lew, J., Winkfein, R.J., Paudel, H.K., and Wang, J.H. (1992). Brain proline-directed protein kinase is a neurofilament kinase which displays high sequence homology to p34cdc2. J. Biol. Chem. *267*, 25922–25926.
5. Meyerson, M., Enders, G.H., Wu, C.L., Su, L.K., Gorka, C., Nelson, C., Harlow, E., and Tsai, L.H. (1992). A family of human cdc2-related protein kinases. EMBO J. *11*, 2909–2917.
6. Tsai, L.H. (2003). The role of cyclin-dependent kinase 5 in brain development abd degeneration. Cell. Mol. Biol. Lett. *8*, 546–547.
7. Tsai, L.H., Takahashi, T., Caviness, V.S., Jr., and Harlow, E. (1993). Activity and expression pattern of cyclin-dependent kinase 5 in the embryonic mouse nervous system. Development *119*, 1029–1040.
8. Nguyen, M.D., and Julien, J.P. (2003). Cyclin-dependent kinase 5 in amyotrophic lateral sclerosis. Neurosignals *12*, 215–220.
9. Lau, L.F., and Ahlijanian, M.K. (2003). Role of cdk5 in the pathogenesis of Alzheimer's disease. Neurosignals *12*, 209–214.
10. Smith, P.D., Crocker, S.J., Jackson-Lewis, V., Jordan-Sciutto, K.L., Hayley, S., Mount, M.P., O'Hare, M.J., Callaghan, S., Slack, R.S., Przedborski, S., et al. (2003). Cyclin-dependent kinase 5 is a mediator of dopaminergic neuron loss in a mouse model of Parkinson's disease. Proc. Natl. Acad. Sci. USA *100*, 13650–13655.
11. Bu, B., Li, J., Davies, P., and Vincent, I. (2002). Deregulation of cdk5, hyperphosphorylation, and cytoskeletal pathology in the Niemann-Pick type C murine model. J. Neurosci. *22*, 6515–6525.
12. Wang, J., Liu, S., Fu, Y., Wang, J.H., and Lu, Y. (2003). Cdk5 activation induces hippocampal CA1 cell death by directly phosphorylating NMDA receptors. Nat. Neurosci. *6*, 1039–1047.
13. Shelton, S.B., and Johnson, G.V. (2004). Cyclin-dependent kinase-5 in neurodegeneration. J. Neurochem. *88*, 1313–1326.
14. Paudel, H.K., Lew, J., Ali, Z., and Wang, J.H. (1993). Brain proline-directed protein kinase phosphorylates tau on sites that are abnormally phosphorylated in tau associated with Alzheimer's paired helical filaments. J. Biol. Chem. *268*, 23512–23518.
15. Baumann, K., Mandelkow, E.M., Biernat, J., Piwnica-Worms, H., and Mandelkow, E. (1993). Abnormal Alzheimer-like phosphorylation of tau-protein by cyclin-dependent kinases cdk2 and cdk5. FEBS Lett. *336*, 417–424.
16. Pei, J.J., Grundke-Iqbal, I., Iqbal, K., Bogdanovic, N., Winblad, B., and Cowburn, R.F. (1998). Accumulation of cyclin-dependent kinase 5 (cdk5) in neurons with early stages of Alzheimer's disease neurofibrillary degeneration. Brain Res. *797*, 267–277.
17. Augustinack, J.C., Schneider, A., Mandelkow, E.M., and Hyman, B.T. (2002). Specific tau phosphorylation sites correlate with severity of neuronal cytopathology in Alzheimer's disease. Acta Neuropathol. (Berl.) *103*, 26–35.
18. Cruz, J.C., Tseng, H.C., Goldman, J.A., Shih, H., and Tsai, L.H. (2003). Aberrant Cdk5 activation by p25 triggers pathological events leading to neurodegeneration and neurofibrillary tangles. Neuron *40*, 471–483.
19. Noble, W., Olm, V., Takata, K., Casey, E., Mary, O., Meyerson, J., Gaynor, K., LaFrancois, J., Wang, L., Kondo, T., et al. (2003). Cdk5 is a key factor in tau aggregation and tangle formation in vivo. Neuron *38*, 555–565.
20. Patrick, G.N., Zukerberg, L., Nikolic, M., de la Monte, S., Dikkes, P., and Tsai, L.H. (1999). Conversion of p35 to p25 deregulates Cdk5 activity and promotes neurodegeneration. Nature *402*, 615–622.
21. Lee, M.S., Kwon, Y.T., Li, M., Peng, J., Friedlander, R.M., and Tsai, L.H. (2000). Neurotoxicity induces cleavage of p35 to p25 by calpain. Nature *405*, 360–364.
22. Kusakawa, G., Saito, T., Onuki, R., Ishiguro, K., Kishimoto, T., and Hisanaga, S. (2000). Calpain-dependent proteolytic cleavage of the p35 cyclin-dependent kinase 5 activator to p25. J. Biol. Chem. *275*, 17166–17172.

23. Tarricone, C., Dhavan, R., Peng, J., Areces, L.B., Tsai, L.H., and Musacchio, A. (2001). Structure and regulation of the CDK5-p25(nck5a) complex. Mol. Cell *8*, 657–669.
24. Jeffrey, P.D., Russo, A.A., Polyak, K., Gibbs, E., Hurwitz, J., Massague, J., and Pavletich, N.P. (1995). Mechanism of CDK activation revealed by the structure of a cyclinA-CDK2 complex. Nature *376*, 313–320.
25. Fischer, P.M. (2001). Recent advances and new directions in the discovery and development of cyclin-dependent kinase inhibitors. Curr. Opin. Drug Discov. Devel. *4*, 623–634.
26. Knockaert, M., Greengard, P., and Meijer, L. (2002). Pharmacological inhibitors of cyclin-dependent kinases. Trends Pharmacol. Sci. *23*, 417–425.
27. Sielecki, T.M., Boylan, J.F., Benfield, P.A., and Trainor, G.L. (2000). Cyclin-dependent kinase inhibitors: useful targets in cell cycle regulation. J. Med. Chem. *43*, 1–18.
28. Garrett, M.D., and Fattaey, A. (1999). CDK inhibition and cancer therapy. Curr. Opin. Genet. Dev. *9*, 104–111.
29. Gray, N., Detivaud, L., Doerig, C., and Meijer, L. (1999). ATP-site directed inhibitors of cyclin-dependent kinases. Curr. Med. Chem. *6*, 859–875.
30. Meijer, L., Leclerc, S., and Leost, M. (1999). Properties and potential-applications of chemical inhibitors of cyclin-dependent kinases. Pharmacol. Ther. *82*, 279–284.
31. Leost, M., Schultz, C., Link, A., Wu, Y.Z., Biernat, J., Mandelkow, E.M., Bibb, J.A., Snyder, G.L., Greengard, P., Zaharevitz, D.W., et al. (2000). Paullones are potent inhibitors of glycogen synthase kinase-3beta and cyclin-dependent kinase 5/p25. Eur. J. Biochem. *267*, 5983–5994.
32. Mettey, Y., Gompel, M., Thomas, V., Garnier, M., Leost, M., Ceballos-Picot, I., Noble, M., Endicott, J., Vierfond, J.M., and Meijer, L. (2003). Aloisines, a new family of CDK/GSK-3 inhibitors. SAR study, crystal structure in complex with CDK2, enzyme selectivity, and cellular effects. J. Med. Chem. *46*, 222–236.
33. Kim, K.S., Kimball, D., Cai, Z.W., Rawlin, D.B., Misra, R.N., Ross, M.A., Webster, K.R., Hunt, J.T., and Han, W.C. July 2001. Aminothiazole inhibitors of cyclin dependent kinases. U.S. patent 6262096 B1.
34. Meijer, L., Thunnissen, A.M., White, A.W., Garnier, M., Nikolic, M., Tsai, L.H., Walter, J., Cleverley, K.E., Salinas, P.C., Wu, Y.Z., et al. (2000). Inhibition of cyclin-dependent kinases, GSK-3beta and CK1 by hymenialdisine, a marine sponge constituent. Chem. Biol. *7*, 51–63.
35. De Azevedo, W.F., Leclerc, S., Meijer, L., Havlicek, L., Strnad, M., and Kim, S.H. (1997). Inhibition of cyclin-dependent kinases by purine analogues: crystal structure of human cdk2 complexed with roscovitine. Eur. J. Biochem. *243*, 518–526.
36. Meijer, L., and Kim, S.H. (1997). Chemical inhibitors of cyclin-dependent kinases. Methods Enzymol. *283*, 113–128.
37. Meijer, L., and Raymond, E. (2003). Roscovitine and other purines as kinase inhibitors. From starfish oocytes to clinical trials. Acc. Chem. Res. *36*, 417–425.
38. Hoessel, R., Leclerc, S., Endicott, J.A., Nobel, M.E., Lawrie, A., Tunnah, P., Leost, M., Damiens, E., Marie, D., Marko, D., et al. (1999). Indirubin, the active constituent of a Chinese antileukaemia medicine, inhibits cyclin-dependent kinases. Nat. Cell Biol. *1*, 60–67.
39. Mapelli, M., Massimiliano, L., Crovace, C., Seeliger, M.A., Tsai, L.H., Meijer, L., and Musacchio, A. (2005). Mechanism of CDK5/p25 binding by CDK inhibitors. J. Med. Chem. *48*, 671–679.
40. Ahn, J.S., Musacchio, A., Mapelli, M., Ni, J., Scinto, L., Stein, R., Kosik, K.S., and Yeh, L.A. (2004). Development of an assay to screen for inhibitors of tau phosphorylation by cdk5. J. Biomol. Screen. *9*, 122–131.
41. Clare, P.M., Poorman, R.A., Kelley, L.C., Watenpaugh, K.D., Bannow, C.A., and Leach, K.L. (2001). The cyclin-dependent kinases cdk2 and cdk5 act by a random, anticooperative kinetic mechanism. J. Biol. Chem. *276*, 48292–48299.
42. Xie, Z., Sanada, K., Samuels, B.A., Shih, H., and Tsai, L.H. (2003). Serine 732 phosphorylation of FAK by Cdk5 is important for microtubule organization, nuclear movement, and neuronal migration. Cell *114*, 469–482.
43. Strocchi, P., Pession, A., and Dozza, B. (2003). Up-regulation of cDK5/p35 by oxidative stress in human neuroblastoma IMR-32 cells. J. Cell. Biochem. *88*, 758–765.
44. Hashiguchi, M., Saito, T., Hisanaga, S., and Hashiguchi, T. (2002). Truncation of CDK5 activator p35 induces intensive phosphorylation of Ser202/Thr205 of human tau. J. Biol. Chem. *277*, 44525–44530.
45. Scott, C.W., Spreen, R.C., Herman, J.L., Chow, F.P., Davison, M.D., Young, J., and Caputo, C.B. (1993). Phosphorylation of recombinant tau by cAMP-dependent protein kinase. Identification of phosphorylation sites and effect on microtubule assembly. J. Biol. Chem. *268*, 1166–1173.
46. Otwinowski, Z., and Minor, W. (1997). Processing of X-ray diffraction data collected in oscillation mode. Methods Enzymol. *276*, 307–325.
47. Navaza, J. (2001). Implementation of molecular replacement in AMoRe. Acta Crystallogr. D Biol. Crystallogr. *57*, 1367–1372.
48. Lamzin, V.S., and Wilson, K.S. (1997). Automated refinement for protein crystallography. Methods Enzymol. *277*, 1–10.
49. van Aalten, D.M., Bywater, R., Findlay, J.B., Hendlich, M., Hooft, R.W., and Vriend, G. (1996). PRODRG, a program for generating molecular topologies and unique molecular descriptors from coordinates of small molecules. J. Comput. Aided Mol. Des. *10*, 255–262.
50. Brunger, A.T., Adams, P.D., Clore, G.M., DeLano, W.L., Gros, P., Grosse-Kunstleve, R.W., Jiang, J.S., Kuszewski, J., Nilges, M., Pannu, N.S., et al. (1998). Crystallography & NMR system: a new software suite for macromolecular structure determination. Acta Crystallogr. D *54*, 905–921.
51. Collaborative Computational Project, N. (1994). The CCP4 suite: programs for protein crystallography. Acta Crystallogr. D *50*, 760–763.
52. Brunger, A.T., and Karplus, M. (1988). Polar hydrogen positions in proteins: empirical energy placement and neutron diffraction comparison. Proteins *4*, 148–156.
53. Brooks, B.R. (1983). CHARMM: a program for macromolecular energy, minimization, and dynamics calculations. J. Comput. Chem. *4*, 187–217.
54. Momany, F.A., and Rone, R. (1992). Validation of the general-purpose QUANTA(R)3.2/CHARMM(R) force-field. J. Comput. Chem. *13*, 888–900.
55. Frisch, M.J. (1995). Gaussian98, Revision A.7. (http://www.gaussian.com).
56. Bayly, C.I., Cieplak, P., Cornell, W.D., and Kollman, P.A. (1993). A well-behaved electrostatic potential-based method using charge restraints for deriving atomic charges—the RESP model. J. Phys. Chem. *97*, 10269–10280.
57. Green, D.F., and Tidor, B. (2003a). Evaluation of ab initio charge determination methods for use in continuum solvation calculations. J. Phys. Chem. *107*, 10261–10273.
58. McLachlan, A.D. (1982). Rapid comparison of protein structures. Acta Crystallogr. *A38*, 871–873.
59. Lee, L.P., and Tidor, B. (1997). Optimization of electrostatic binding free energy. J. Chem. Phys. *106*, 8681–8690.
60. Kangas, E., and Tidor, B. (1998). Optimizing electrostatic affinity in ligand-receptor binding: theory, computation, and ligand properties. J. Chem. Phys. *109*, 7522–7544.
61. Lee, L.P., and Tidor, B. (2001). Optimization of binding electrostatics: charge complementarity in the barnase-barstar protein complex. Protein Sci. *10*, 362–377.
62. Chu, J.W., Trout, B.L., and Brooks, B.R. (2003). A super-linear minimization scheme for the nudged elastic band method. J. Chem. Phys. *24*, 12708–12717.
63. Gilson, M.K., and Honig, B. (1988). Calculation of the total electrostatic energy of a macromolecular system: solvation energies, binding energies, and conformational analysis. Proteins *4*, 7–18.
64. Gilson, M.K., Sharp, K.A., and Honig, B.H. (1988). Calculating the electrostatic potential of molecules in solution—method and error assessment. J. Comput. Chem. *9*, 327–335.
65. Sharp, K.A., and Honig, B. (1990). Electrostatic interactions in macromolecules: theory and applications. Annu. Rev. Biophys. Biophys. Chem. *19*, 301–332.
66. Midelfort, K.S., Hernandez, H.H., Lippow, S.M., Tidor, B., Drennan, C.L., and Wittrup, K.D. (2004). Substantial energetic im-

provement with minimal structural perturbation in a high affinity mutant antibody. J. Mol. Biol. *343*, 685–701.
67. Sitkoff, K.A., Sharp, K.A., and Honig, B. (1994). Accurate calculation of hydration free energies using macroscopic solvent models. J. Phys. Chem. *98*, 1978–1988.
68. Green, D.F., and Tidor, B. (2003b). Evaluation of electrostatic interactions. In Current Protocols in Bioinformatics, Unit 8.3, Andreas D. Baxevanis and Daniel B. Davison, eds. (New York: John Wiley & Sons).
69. Vanderbei, R.J. (1999a). LOQO: An interior-point code for quadratic programming. Optimization Methods Software *12*, 451–454.
70. Vanderbei, R.J. (1999b). LOQO User's Manual—version 3.10. Optimization Methods and Software *12*, 485–514.
71. Humphrey, W., Dalke, A., and Schulten, K. (1996). VMD: visual molecular dynamics. J. Mol. Graph. *14*, 27–38.
72. Merritt, E.A., and Bacon, D.J. (1997). Raster3D: photorealistic molecular graphics. Methods Enzymol. *277*, 505–524.